GX 9+9: VARIABILITY OF THE X-RAY ORBITAL MODULATION

Citation: Harris, Robert J., Alan M. Levine, Martin Durant, Albert K. H. Kong, Phil Charles, and Tariq Shahbaz. "GX 9+9: VARIABILITY OF THE X-RAY ORBITAL MODULATION." The Astrophysical Journal 696, no. 2 (April 28, 2009): 1987–1997. © 2009 American Astronomical Society.

As Published: http://dx.doi.org/10.1088/0004-637x/696/2/1987

Publisher: Institute of Physics/American Astronomical Society

Persistent URL: http://hdl.handle.net/1721.1/96230

Version: Final published version: final published article, as it appeared in a journal, conference proceedings, or other formally published context

The Astrophysical Journal, 696:1987–1997, 2009 May 10 doi:10.1088/0004-637X/696/2/1987

GX 9+9: VARIABILITY OF THE X-RAY ORBITAL MODULATION

Robert J. Harris[1,6], Alan M. Levine[2], Martin Durant[3], Albert K. H. Kong[4], Phil Charles[5], and Tariq Shahbaz[3]
[1] Department of Physics and Kavli Institute for Astrophysics and Space Research, Massachusetts Institute of Technology, Cambridge, MA 02139, USA; rjharris@cfa.harvard.edu
[2] Kavli Institute for Astrophysics and Space Research, Massachusetts Institute of Technology, Cambridge, MA 02139, USA; aml@space.mit.edu
[3] Instituto de Astrofísica de Canarias, La Laguna, Tenerife, Spain
[4] Department of Physics and Institute of Astronomy, National Tsing Hua University, Hsinchu, Taiwan
[5] South African Astronomical Observatory, P.O. Box 9, Observatory 7935, South Africa
Received 2008 June 5; accepted 2009 February 23; published 2009 April 28

ABSTRACT

Results of observations of the Galactic bulge X-ray source GX 9+9 by the All-Sky Monitor (ASM) and Proportional Counter Array (PCA) onboard the *Rossi X-ray Timing Explorer* are presented. The ASM results show that the 4.19 hr X-ray periodicity first reported by Hertz and Wood in 1987 was weak or not detected for most of the mission prior to late 2004, but then became strong and remained strong for approximately two years after which it weakened considerably. When the modulation at the 4.19 hr period is strong, it appears in folded light curves as an intensity dip over $\lesssim$30% of a cycle and is distinctly nonsinusoidal. A number of PCA observations of GX 9+9 were performed before the appearance of strong modulation; two were performed in 2006 during the epoch of strong modulation. Data obtained from the earlier PCA observations yield, at best, limited evidence of the presence of phase-dependent intensity changes, while the data from the later observations confirm the presence of flux minima with depths and phases compatible with those apparent in folded ASM light curves. Light curves from a *Chandra* observation of GX 9+9 performed in the year 2000 prior to the start of strong modulation show the possible presence of shallow dips at the predicted times. Optical observations performed in 2006 while the X-ray modulation was strong do not show an increase in the degree of modulation at the 4.19 hr period. Implications of the changes in modulation strength in X-rays and other observational results are considered.

Key words: stars: individual (GX 9+9) – X-rays: binaries

1. INTRODUCTION

The bright Galactic X-ray source GX 9+9 has the characteristics of a low-mass X-ray binary (LMXB) system and particularly of the atoll-type LMXB subclass that is defined by the behavior of the source X-ray energy and power density spectra (PDS; Mayer et al. 1970; Schulz et al. 1989; Hasinger & van der Klis 1989; van der Klis 2006). A periodicity of 4.19 ± 0.02 hr in its X-ray flux was discovered using *HEAO* A-1 data by Hertz & Wood (1988). The periodic component was weak; its strength, in terms of the amplitude of the best-fit sinusoid, was approximately 4% of the average flux. Hertz & Wood interpreted the modulation as indicative of the orbital period of the binary system. Under the assumption that the system consists of a 1.4 $M_\odot$ neutron star and a Roche-lobe-filling lower-main-sequence star, they inferred that the latter is an early M dwarf with mass $M \approx 0.2$–$0.45\ M_\odot$ and radius $R \approx 0.3$–$0.6\ R_\odot$. They used these values to put an upper bound on the orbital inclination of $i \lesssim 63^\circ$ but, as noted by Schaefer (1990), apparently they calculated R_2/a incorrectly; the correct bound on the inclination is $i \lesssim 77^\circ$.

Schaefer (1990) found variations of the brightness of the optical counterpart of GX 9+9 at essentially the same period, viz., 4.198 ± 0.009 hr. The modulation amplitude was about 0.19 mag peak to peak in the B band in 1987 and appeared to be somewhat larger in 1988. In the latter observations, the amplitude was roughly the same in each of the B, V, and R bands.

Kong et al. (2006) carried out nearly simultaneous observations of GX 9+9 in 1999 in the optical at the Radcliffe Telescope of the South African Astronomical Observatory and in X-rays with the Proportional Counter Array (PCA) instrument on the *Rossi X-ray Timing Explorer* (*RXTE*). They found that modulation at the presumed orbital period was clearly present in the optical, but no modulation at that period was apparent in either the 2–3.5 keV or the 9.7–16 keV photon energy bands. Kong et al. also reviewed archival data from a 14.4 hr observation of GX 9+9 made with *EXOSAT* in 1983, a 6.6 hr observation made with *ASCA* in 1994, and a 6.4 hr observation made with *BeppoSAX* in 2000, but did not find significant evidence of the 4.19 hr periodicity.

Cornelisse et al. (2007) obtained phase-resolved spectra of the optical counterpart in 2004 May and found emission lines which comprise components with differing radial velocity variations that must originate in different places in the binary system, one of which is likely to be the X-ray-illuminated face of the secondary. The 4.19 hr period is clearly evident in the radial velocity variations. Thus, these observations strongly confirm that this is the orbital period. The phenomenon was most clear in the He II λ4686 line but was also evident in the Bowen blend and around Hβ. Following early reports of the detection of the 4.19 hr period in the *RXTE* All-Sky Monitor (ASM) data and variation of the strength of the modulation (Levine et al. 2006; Levine & Corbet 2006), Cornelisse et al. (2007) used the ASM data to estimate the period and time of X-ray minimum. They were then able to relate the time of X-ray minimum, the phases of the radial velocity variations, and the variation of the brightness of the optical counterpart in the blue continuum to each other. They also derived model-dependent lower and upper limits on the binary mass ratio and on the orbital velocity of the secondary.

Herein we present evidence that the X-ray photometric signature of the (presumed) binary orbit of GX 9+9 has undergone dramatic changes over the ∼12 years that the source

[6] Current address: Center for Astrophysics, 60 Garden Street, Cambridge, MA 02138, USA.

has been monitored with the ASM. In addition to describing the results of our analysis of ASM data, we present results of analysis of a number of PCA observations, of an observation of GX 9+9 performed in 2000 with the *Chandra X-ray Observatory*, and of optical observations performed in 2006. In Section 2, we describe the instrumentation, observations, and the results from the observations. In Section 3, we summarize our results, suggest for the first time in the literature, to our knowledge, that the observed modulation is closely related to the dipping seen in other LMXBs, and discuss in general the possible implications of this investigation.

2. INSTRUMENTATION, OBSERVATIONS, AND RESULTS

2.1. ASM Observations and Results

The ASM consists of three Scanning Shadow Cameras (SSCs) mounted on a rotating Drive Assembly (Levine et al. 1996). Approximately 50,000 measurements of the intensity of GX 9+9, each from a 90 s exposure with a single SSC, were obtained from the beginning of the *RXTE* mission in early 1996 through 2007. A single exposure yields intensity estimates in each of the three spectral bands which nominally correspond to photon energy ranges of 1.5–3, 3–5, and 5–12 keV with sensitivity of a few SSC counts s^{-1} (the Crab Nebula produces intensities of 27, 23, and 25 SSC counts s^{-1} in the three bands, respectively). For the analyses presented herein, we use observation times that have been adjusted so as to represent times at the barycenter of the solar system.

The properties of the three SSCs have evolved over the ∼12 years of operation of the ASM. SSC 1 (of SSCs 1–3) has a slow gas leak that has resulted in the photon energy to pulse height conversion gain increasing by about 10% yr^{-1} or about a factor of 3 over 12 years. A number of proportional counter cells in SSCs 2 and 3 have become permanently inoperational at various times since the beginning of the mission because of catastrophic high voltage breakdown events that removed the thin carbon layer on the carbon-coated quartz fiber anodes of those cells. In all three detectors, the properties of the carbon coatings of the anodes have gradually changed. These effects are, to first order, removed in the course of the standard analysis procedure of the raw ASM data by the ASM team that produces the light curve files. The procedure is adjusted so that the observed intensities of the Crab Nebula in the four energy bands are more or less stable and close to the intensities seen in SSC 1 in 1996 March. The results in the 5–12 keV energy band from SSC 1 at late times are corrected by the largest factors since most events due to photons in this energy range in this SSC are not usable because they are saturated in the amplifiers. Thus, in preparing light curves from GX 9+9 for this paper, we compared the results from SSC 1 with those from SSCs 2 and 3. We found that the SSC 1 light curve deviated negligibly from that produced from SSCs 2 and 3 before MJD 54,200 and after that time gradually increased up to ∼1 SSC counts s^{-1} above the intensities derived from SSCs 2 and 3 by MJD 54,600.

The ASM light curve of GX 9+9 is shown in Figure 1. It was made using data from all three SSCs for times prior to MJD 54,200, and from only SSCs 2 and 3 for times after MJD 54,200. It shows a relatively strong source that varies on timescales of years. The intensity changes include a distinct sinusoidal-like component superimposed on a slowly increasing baseline. No spectral changes are apparent in the ASM light curves beyond small differences that are likely to be of instrumental origin.

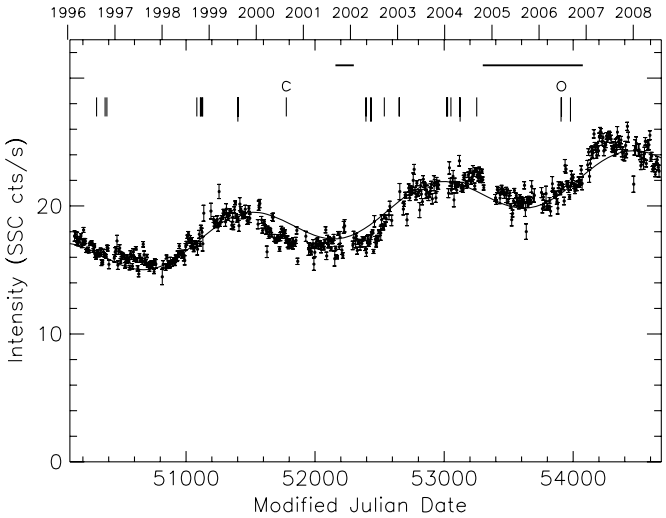

Figure 1. ASM 1.5–12 keV light curve of GX 9+9 with measurements averaged in contiguous 7 day time bins. For times earlier than MJD 54,200, the measurements include data from all three SSCs. After MJD 54,200, this light curve is based only on data from SSCs 2 and 3. Those weighted average measurements with estimated uncertainties larger than 0.65 SSC counts s^{-1} are not shown. For reference, the Crab Nebula intensity in the same band corresponds to 75 SSC counts s^{-1}. The smooth curve is the best-fit function consisting of a constant, linear term, and sinusoid (see the text). The period of the sinusoid is 1473 days. The vertical indicator marks show the times of various observations. The marks without letters show the times of the 29 PCA observations of GX 9+9 that were longer than 1 hr in duration; the longer marks show the times of the PCA observations with exposures greater than 4 hr. The time of the *Chandra* observation is denoted with a "C"; the time of the optical observations reported herein are denoted with an "O." The heavy horizontal indicator bars approximately mark the times when the X-ray modulation was easily detectable.

To obtain a quantitative description of the long-period sinusoidal-like component, we fit the light curve shown in Figure 1 with the simple function

$$F_x = a + b(t - 50100) + c\sin(2\pi t/P_{\rm long}) + d\cos(2\pi t/P_{\rm long}), \quad (1)$$

where F_x is the model 1.5–12 keV X-ray intensity, t is the time as a Modified Julian Date, $P_{\rm long}$ is the to-be-determined period of the sinusoid, and a, b, c, and d are also parameters to be determined. The best-fit curve, with $P_{\rm long} = 1473$ days, is shown superimposed on the ASM light curve in Figure 1. The fit is not good, i.e., the value of the reduced χ^2 statistic is much greater than 1. Given this fit quality and the small number of cycles of the sinusoid, we cannot confidently conclude that the long-term light curve contains a periodic component that is coherent over more than ∼3 cycles. Nonetheless, the form of the light curve suggests that some type of quasi-periodic long-term variability may be present.

In the early stages of a search for periodicities in ASM data using advanced analysis techniques, Shivamoggi (2005) applied the first of two primary strategies of improving the sensitivity of the search to high-frequency variations, and detected the 4.19 hr periodicity in the ASM light curve of GX 9+9. The first strategy involves the use of appropriate weights such as the reciprocals of the variances in Fourier and other types of analyses since the individual ASM measurements have a wide range of associated uncertainties. The second strategy stems from the fact that the observations of the source are obtained with a low duty cycle, i.e., the window function is sparse (and complex). The properties of the window function, in combination with the presence of slow variations of the source intensity, act to hinder the detection

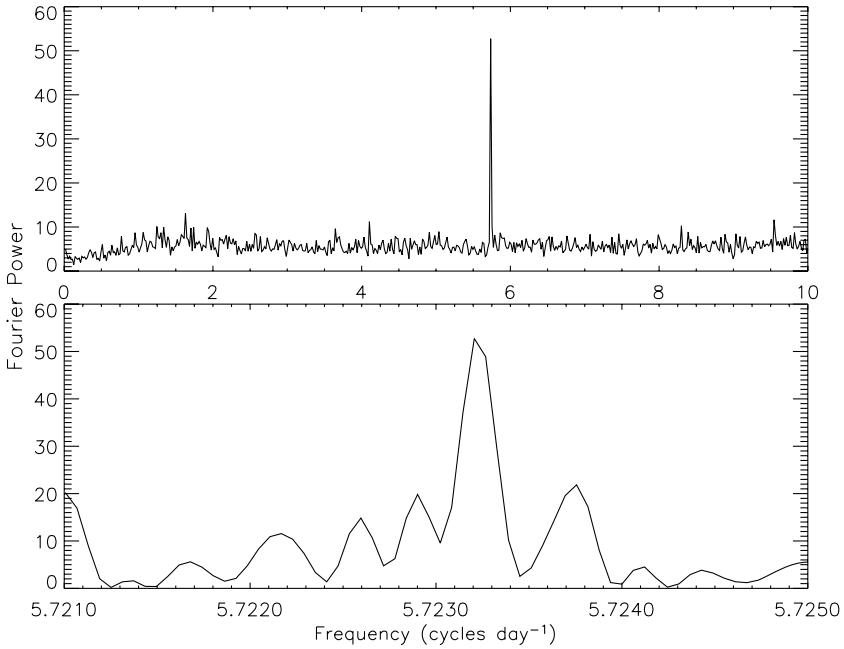

Figure 2. PDS of a 1.5–12 keV ASM light curve of GX 9+9 that had been modified to remove variability on timescales longer than ∼1 day (see the text). The original FFT was oversampled and had approximately two million frequencies from 0 cycles day^{-1} to the Nyquist frequency of 144 cycles day^{-1}. Upper panel: a rebinned PDS in which the number of frequency bins was reduced by a factor of 300 by using the maximum power in each contiguous set of 300 frequency bins in the original PDS as the power of the corresponding bin in the rebinned PDS. Lower panel: a portion of the original PDS. In both panels, the power is normalized relative to the PDS-wide average.

of variations on short timescales. The window function PDS has substantial power at high frequencies, e.g., 1 cycle day^{-1} and 1 cycle per spacecraft orbit (∼95 minute period). Since the data may be regarded as the product of a (hypothetical) continuous set of source intensity measurements with the window function, a Fourier transform of the data is equivalent to the convolution of a transform of a continuous set of intensity measurements with the window function transform. The high-frequency structure in the window function transform acts to spread power at low frequencies in the source intensity to high frequencies in the calculated transform (or, equivalently, the PDS). This effectively raises the noise level at high frequencies.

In our analysis, the sensitivity to high-frequency variations is enhanced by subtracting a smoothed version of the light curve from the unsmoothed light curve. To perform the smoothing, we do not simply convolve a box function with the binned light curve data since that would not yield any improvement in the noise level at high frequencies. Rather, we ignore bins which do not contain any actual measurements and we use weights based on estimates of the uncertainties in the individual measurements to compute the smoothed light curve. The "box" used in the smoothing had a length of 0.9 day, so the smoothed light curve displayed only that variability with Fourier components at frequencies below ∼1 day^{-1}. The smoothed light curve was subtracted from the unsmoothed light curve, and the difference light curve was Fourier transformed. The results are illustrated in Figure 2. The center frequency and width (half-width at half-maximum) of the peak correspond to a period of 4.19344 ± 0.00007 hr (0.1747267 ± 0.0000029 days).

To investigate the time variability of the orbital modulation, we folded the barycenter-corrected light curves for each of the 30 equal time intervals at the 4.19344 hr period; see Figure 3 and Table 1. The figure shows that the modulation of GX 9+9 was weak during the first five years of the mission. It then seems to have appeared at a somewhat detectable level for a brief time in late 2001 and/or early 2002 (panel 15). In late 2004 or early 2005 the modulation grew stronger, and it stayed strong until late in 2006 when it began to decrease in strength. In the final two panels, the modulation is not present at a significant level. We note that the interval of relatively strong modulation, i.e., approximately from MJD 53,300 to MJD 54,100, corresponds to a time interval in which the overall intensity is below the levels given by an interpolation from earlier to later times (see Figure 1).

In Figure 4, we show folded light curves for the 1.5–3, 3–5, and 5–12 keV photon-energy bands as well as for the overall 1.5–12 keV band for the time interval of MJD 53,300 through MJD 54,075 when the modulation was strongest. The modulation appears to be largely energy-independent and, in particular, the spectrum of GX 9+9 does not significantly change during the dips. This is confirmed by the hardness ratios computed from these folded light curves by taking bin-wise ratios as shown on the right-hand side of Figure 4.

We have used the folded light curves to determine the epoch of X-ray minimum, i.e., the time corresponding to the centroid of the diplike feature. The best linear fit to the times of the minima is given by

$$T_{\rm min} = 53382.959 \pm 0.003 + (0.1747267 \pm 0.0000029)N, \quad (2)$$

where the times are Modified Julian Dates in the UTC time system and apply at the barycenter of the solar system. One should note that, as per Figure 4, dip activity may occur within ±0.15 cycles (= ±0.63 hr) of the times of minimum. It must be pointed out that this ephemeris is not consistent with that of Cornelisse et al. (2007); their time of minimum occurs at 0.24 ± 0.04 cycles relative to a time of minimum given by this equation.

2.2. PCA Observations and Results

The PCA consists of five mechanically collimated large area Proportional Counter Units (PCUs) and is primarily sensitive to

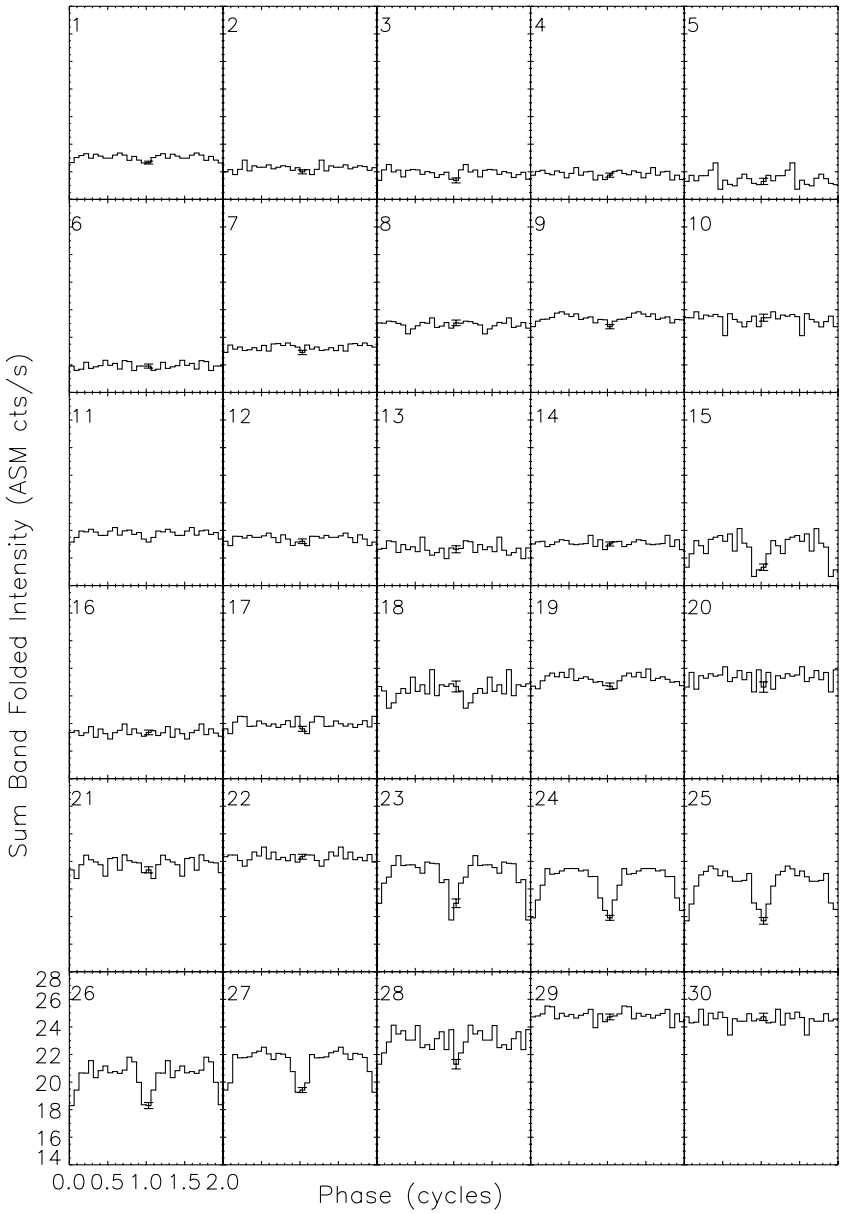

Figure 3. Barycenter-corrected ASM 1.5–12 keV light curves of GX 9+9 from each of the 30 equal-duration time intervals folded using the epoch and period in Equation (2), i.e., MJD 53,382.959 and 4.19344 hr = 0.1747267 days, respectively. Each interval spans ∼144.40 days; dates may be found in Table 1. All vertical axes have the same scale and offset, as do all horizontal axes. The interval numbers are given in the top left corners. Typical $\pm 1\sigma$ uncertainties are shown.

2–60 keV photons (Jahoda et al. 2006, and references therein). A total of 61 observations of GX 9+9 were carried out with the PCA from 1996 through 2004. Only 29 of these were over 1 hr in duration; 17 were over 4 hr; the longest was ∼15 hr. Twelve of the 29 observations were performed in the time period 1996–1999; 17 were performed between 2002 and 2004. In addition, as per our request, a pointed observation of GX 9+9 was carried out on 2006 June 20. One further observation of the source was carried out on 2006 September 1. GX 9+9 typically produced 500–700 counts s^{-1} PCU^{-1} in the 2–12 keV energy band in these observations.

For our periodicity search and X-ray "color" analyses using PCA data, we have used data accumulated in Standard Mode 2 which provides counts in each of the 128 pulse height channels for each PCU for 16 s time intervals. Data accumulated in various event and single-bit modes that provided a time resolution of 500 μs or better were used for our fast-timing analyses. Background has been neglected for most of the timing analyses. However, in the analyses involving X-ray colors, the data have been corrected for both the background as well as gain drifts over the course of the mission. The times of the data have been corrected to the solar system barycenter for all of the analyses presented herein.

In response to the discovery of the strengthening of the orbital modulation in the ASM data (Levine et al. 2006), we searched the pre-2006 archival PCA data for evidence of the 4.19 hr periodicity. In our search we used only the 29 observations that were longer than 1 hr. The total exposure obtained during these observations was ∼460 ks. Since the ASM data show no significant modulation during the times of the observations, we expected to find no evidence of modulation in the PCA data.

We folded the barycenter-corrected data from the 29 observations at each of the periods in a grid of closely spaced values centered on 4.19344 hr. We did this for the energy bands 2–5,

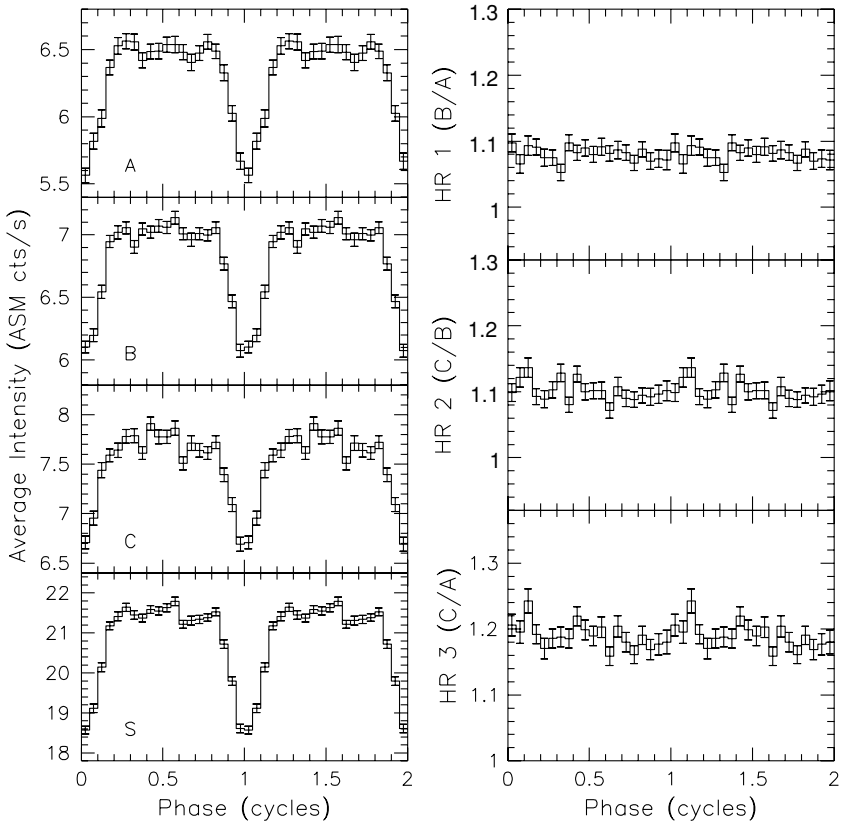

Figure 4. Left: folded barycenter-corrected light curves from ASM observations of GX 9+9 from 2004 October 22 (MJD 53,300) through 2006 December 6 (MJD 54,075). The energy bands are 1.5–3 keV (A), 3–5 keV (B), 5–12 keV (C), and 1.5–12 keV (S). The folding was accomplished using the period and epoch in Equation (2). Right: hardness ratios implied by bin-wise ratios of folded intensities.

5–12, and 12–30 keV. For each folded light curve, we computed a χ^2 statistic based on the hypothesis of no variation as a function of phase and plotted the resulting values against folding period. No significant peaks were found. We also found no significant changes in the color of the source that correlated with the phase of the folds.

This search for periodic modulation was done against a background of variability which tends to be stronger at higher than at lower photon energies. On timescales of 256 s, the rms variability seen in the PCA light curves, expressed as a fraction of the mean count rate, is 3.1% in the 2–6 keV band, 6.4% in the 6–10 keV band, and 9.6% in the 10–16 keV band. On timescales of 24 minutes, the rms is 3.3% in the 2–6 keV band, 5.1% in the 6–10 keV band, and 6.9% in the 10–16 keV band. These results agree roughly with the ASM light curves, which yield a ∼4% rms intrinsic variability in each of the A, B, and C bands. This should be compared to the original variability estimate of Hertz & Wood (1988) who calculated a 4.6% intrinsic source variability in addition to the 3.8% sinusoidal modulation at the orbital period (4.19 hr) in the 0.5–20 keV *HEAO* A-1 light curve.

While the folding analysis did not yield any evidence for persistent modulation that was stable in phase, upon examination of the individual pre-2006 PCA observations, diplike events were evident on rare occasions; they are illustrated in Figures 5 and 6. In the light curve from the observation on 2002 May 1 (Figure 5), the most well defined diplike event is seen near 12.5 hr. A weaker diplike event is seen near 8.3 hr; it is not much more prominent than some other diplike events in this observation. In the light curve from the observation on 2002 June 6 (top panel of Figure 6), narrow dips are evident at about 0.6 and 5.3 hr. The times, orbital phases, and depths of these dips are given in Table 2. Prominent dips are not seen in the light curves from 2002 June 11, merely 5 days later, nor are they evident in the light curves from 2004 April 29. The dips seen on 2002 May 1 and on 2002 June 6 are shorter than the dips seen in the folded ASM light curves. The time of one of these dips is not centered on a time given by Equation (2), but the phases of all four may be consistent with the extent in phase of the dips seen in the folded ASM light curves. We did not find any other particularly noticeable dips in the light curves from any of the other pre-2006 PCA observations that were one or more hours in duration.

As per our request to the *RXTE* Mission Scientist for new observations, GX 9+9 was observed for 10 hr with the PCA (and the High Energy X-Ray Timing Experiment) on 2006 June 20 (MJD 53,906). The results are shown in three different energy bands in Figure 7. According to Equation (2), we find that the times of minimum flux should occur at 6.37 ± 0.22 hr and 10.56 ± 0.22 hr (TT) on 2006 June 20. Indeed, prominent dips in the intensity can be seen close to these predicted times in the two lower energy bands and at the earlier of the two times in the 10–18 keV band. Estimates of the times, orbital phases, and depths of these two dips are given in Table 2 wherein the depths are seen to be more or less independent of energy. It is not clear whether the second of these two dips is less prominent in the 10–18 keV band (Figure 7) because of generally stronger variability at higher than at lower energies or, alternatively, that it actually is less deep and the uncertainty on the depth given in Table 2 is underestimated.

Another pointed observation was done on 2006 September 1 (MJD 53,979). Like that on 2006 June 20, this one also took place during an interval (Figure 3) in which the source exhibited

Table 1
Time Intervals of Figure 3 Panels

Interval	Begin MJD[a]	Begin Date[b]
1	50,135.0	1996 Feb 22
2	50,279.4	1996 Jul 15
3	50,423.8	1996 Dec 6
4	50,568.2	1997 Apr 30
5	50,712.6	1997 Sep 21
6	50,857.0	1998 Feb 13
7	51,001.4	1998 Jul 7
8	51,145.8	1998 Nov 28
9	51,290.2	1999 Apr 22
10	51,434.6	1999 Sep 13
11	51,579.0	2000 Feb 5
12	51,723.4	2000 Jun 28
13	51,867.8	2000 Nov 19
14	52,012.2	2001 Apr 13
15	52,156.6	2001 Sep 4
16	52,301.0	2002 Jan 27
17	52,445.4	2002 Jun 20
18	52,589.8	2002 Nov 11
19	52,734.2	2003 Apr 5
20	52,878.6	2003 Aug 27
21	53,023.0	2004 Jan 19
22	53,167.4	2004 Jun 11
23	53,311.8	2004 Nov 2
24	53,456.2	2005 Mar 27
25	53,600.6	2005 Aug 18
26	53,745.0	2006 Jan 10
27	53,889.4	2006 Jun 3
28	54,033.8	2006 Oct 25
29	54,178.2	2007 Mar 19
30	54,322.6	2007 Aug 10
31[c]	54,467.0	2008 Jan 2

Notes.
[a] Modified Julian Date rounded to one decimal place.
[b] Corresponding to the rounded MJD.
[c] The end of interval 30.

strong modulation. With respect to the time reference used for the right half of Figure 7, Equation (2) predicts times of minimum flux at 11.42 ± 0.25 and 15.61 ± 0.25 hr. In this observation, dips are evident near 11.7 and 15.9 hr. They are most apparent in the 2–6 keV band. The first dip is hardly evident in the 6–10 and 10–18 keV bands, perhaps because of a flare in which the spectral hardness undergoes a large increase. The dip near 15.9 hr is quite evident in both higher energy bands; times, phases, and fractional depths are given in Table 2. The depths of this dip are, like those seen on 2006 June 20, also more or less independent of energy. We have not determined the depths or phase of the dip near 11.7 hr because of its proximity to the flare.

The two dips seen in the 2006 June observation and the second dip seen in the 2006 September observation are comparable in terms of fractional depth with those seen in the folded ASM light curves (see interval 27 in Figure 3), and are, as noted immediately above, energy independent to a good approximation. They are narrower (∼0.05 orbital cycles) than the dips in the folded ASM light curves. The phases of the three dips fall within the extent in phase of the dips in the folded ASM light curves.

After searching the PCA observations for evidence of persistent modulation, we attempted to determine whether or not the characteristics of the source's high-frequency PDS had changed since the increase of modulation. We also attempted to see if any change in the X-ray color-related phenomenology had occurred in tandem with the modulation strength increase. We report on both the fast-timing and color analyses below.

2.3. *Fast-timing Analysis*

Quasi-periodic oscillations (QPOs) are often seen in the X-ray intensities of neutron-star LMXBs (see the review by van der Klis 2006 and references therein). Theoretical considerations suggest that these oscillations are generated in the accretion disks, although there is no consensus on the details of the physical mechanisms causing the oscillations. GX 9+9 has never been reported to exhibit such QPOs (see, e.g., Wijnands et al. 1998). In this respect, it is like the other bright atoll-type GX sources (van der Klis 2006). Because of the discovery of the modulation-strength increase in the source, we reviewed all available PCA observations, but did not find statistically significant QPOs. In particular, the source did not exhibit statistically significant QPOs in the frequency range ∼0.01–1000 Hz during either the 2006 June or 2006 September observations.

2.4. *Color Analysis*

GX 9+9, like the other atoll-type GX sources, generally occupies the upper and lower banana regions in a soft color–hard color diagram (Schulz et al. 1989; Wijnands et al. 1998; van der Klis 2006). We wondered whether the presence of strong modulation would have any impact on the details of the color–color diagram. We used data only from PCU 3 (of PCUs 1–5) for this analysis. The data were corrected for background and gain changes, and then used to make color–color diagrams for both the 2006 June and 2006 September observations. We then compared these with a color–color diagram made from all data from previous PCA observations of GX 9+9. We found no significant differences among the diagrams.

2.5. Chandra *Observations*

Chandra comprises a high angular resolution X-ray telescope and two focal plane cameras along with a pair of transmission diffraction gratings each of which may be placed in the X-ray beam just behind the mirror assembly for spectral observations. The ACIS-S focal plane array, which was used for the observation described below, is composed of four front-illuminated (FI) and two back-illuminated (BI) CCDs configured in a 6 by 1 array. It provides a field of approximately $8' \times 48'$. The on-axis effective area for either the FI or BI CCDs is 340 cm^2 at 1 keV, and the spectral resolution is $E/dE = 20$–50 (1–6 keV) for the FI CCDs and $E/dE = 9$–35 (1–6 keV) for the BI CCDs. See Weisskopf et al. (2002) for further information.

A 20 ks long observation of GX 9+9 was carried out with the Observatory on 2000 August 22 beginning at 05:20:21 UTC (MJD 51,778.2225); the ACIS-S instrument was used as the focal plane camera, and the High-Energy Transmission Grating (HETG) was in the X-ray beam. The zero-order image of GX 9+9 was placed on the back-illuminated CCD S3. The count rate of good events in the dispersed spectra, i.e., not including the counts in the zero-order image, is shown in Figure 8. Only small changes in the rate are evident. Among these changes are two shallow minima with depths of approximately 4% of the mean count rate that are approximately 15 ks apart. These times are consistent with the times of X-ray minimum according to Equation (2).

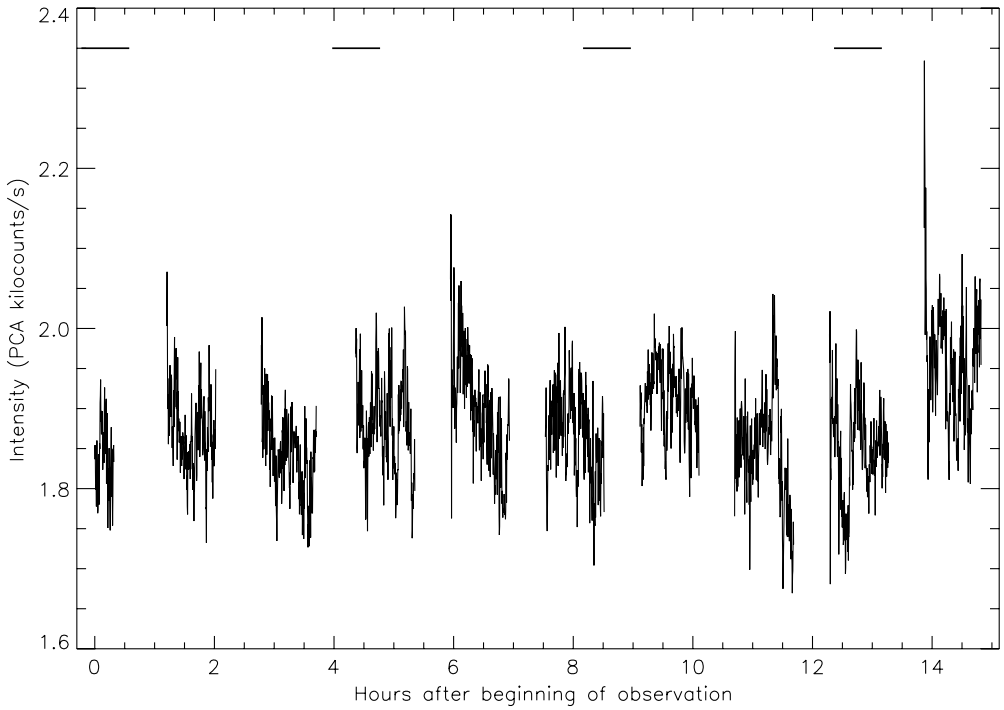

Figure 5. Light curve of counts in the 2–6 keV band of GX 9+9 obtained from a PCA observation beginning at 13:42:20 UTC on 2002 May 1 (MJD 52,395; observation ID 70022-02-01-01). The horizontal bars indicate the times of X-ray minimum according to Equation (2). Note that there is one possible dip at ∼8.3 hr which is consistent with the phase of the ASM dip and there is another more noticeable dip at 12.5 hr.

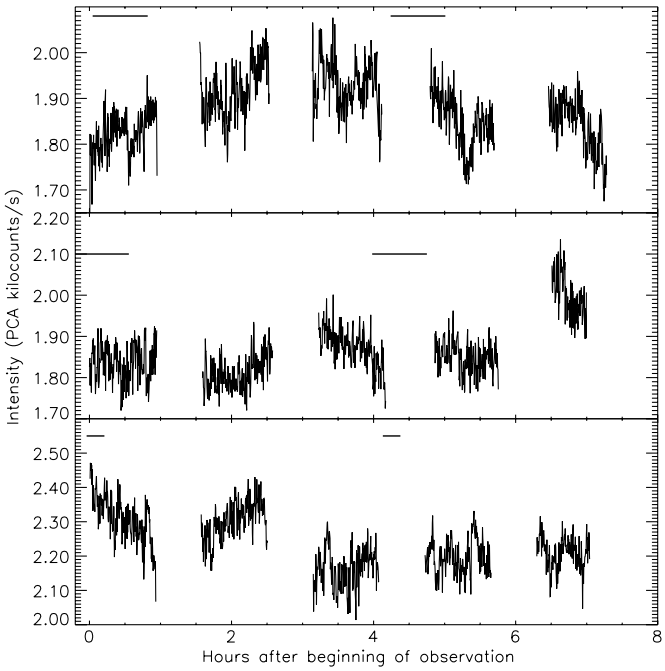

Figure 6. PCA count rates in the 2–6 keV band during three observations of GX 9+9. Top: the observation beginning at 9:06:20 on 2002 June 6 (MJD 52,431; observation ID 70022-02-05-00). Middle: that beginning at 10:58:36 on 2002 June 11 (MJD 52,436; ID 70022-02-06-00. Bottom: that beginning at 17:03:08 on 2004 April 29 (MJD 53,124; ID 70022-02-09-00). The horizontal bars indicate the times of X-ray minimum according to Equation (2).

2.6. Optical Observations

We observed the field of GX 9+9 in 2006 June in white light, i.e., with no filter, with the CCD imaging camera on the 1.9 m Radcliffe Telescope of the South African Astronomical Observatory (SAAO). In order to achieve rapid read-out, we only used a 127 × 96 pixel data area, giving a read-out cycle of 6 s. The observing run was seven nights, of which two were clouded out and two partially affected by poor weather. Seeing was variable, but under 1″ for substantial periods of the three good nights.

These observations were performed not long after the PCA observations of GX 9+9 on 2006 June 20, while the orbital modulation in X-rays was strong (see Figures 3 and 7).

For each image, we subtracted a bias frame and divided by a flat-field image prepared for each night. Since GX 9+9 is located between a bright star and two close fainter stars, aperture photometry does not yield reliable results in the presence of seeing variability. We therefore used the DAOPHOT II software package (Stetson 1987; Stetson et al. 1990) to fit a point-spread function (PSF) to each stellar image; the image of the brightest star served as the PSF and photometric reference. Another star of similar distance from the reference star and similar brightness to GX 9+9 is used as a test of the photometric systematics. It shows a typical uncertainty of 0.01 mag (1 σ) during stable conditions. The photometric results were further selected by rejecting those values which deviated by more than 0.05 mag from a 10 m local average and were then averaged in 1 m time bins. The resulting light curves from the three nights with the best conditions are shown in Figure 9.

The light curves are plotted as a function of X-ray phase in Figure 10. A marked decline in the intensity of the counterpart is apparent late in the observations particularly on the nights of June 23–24 and 24–25. Thus, the tails of the light curves from these nights (shown in red and blue in Figure 10) fall significantly below the other measurements at similar phases. This could easily be an atmospheric effect since the counterpart of GX 9+9 has a relatively blue spectrum compared to most stars deep in the Galactic plane and, thus, may have more blue or UV flux than the comparison star. Furthermore, the field was on the meridian at ∼0.075 days before 0^h UTC during

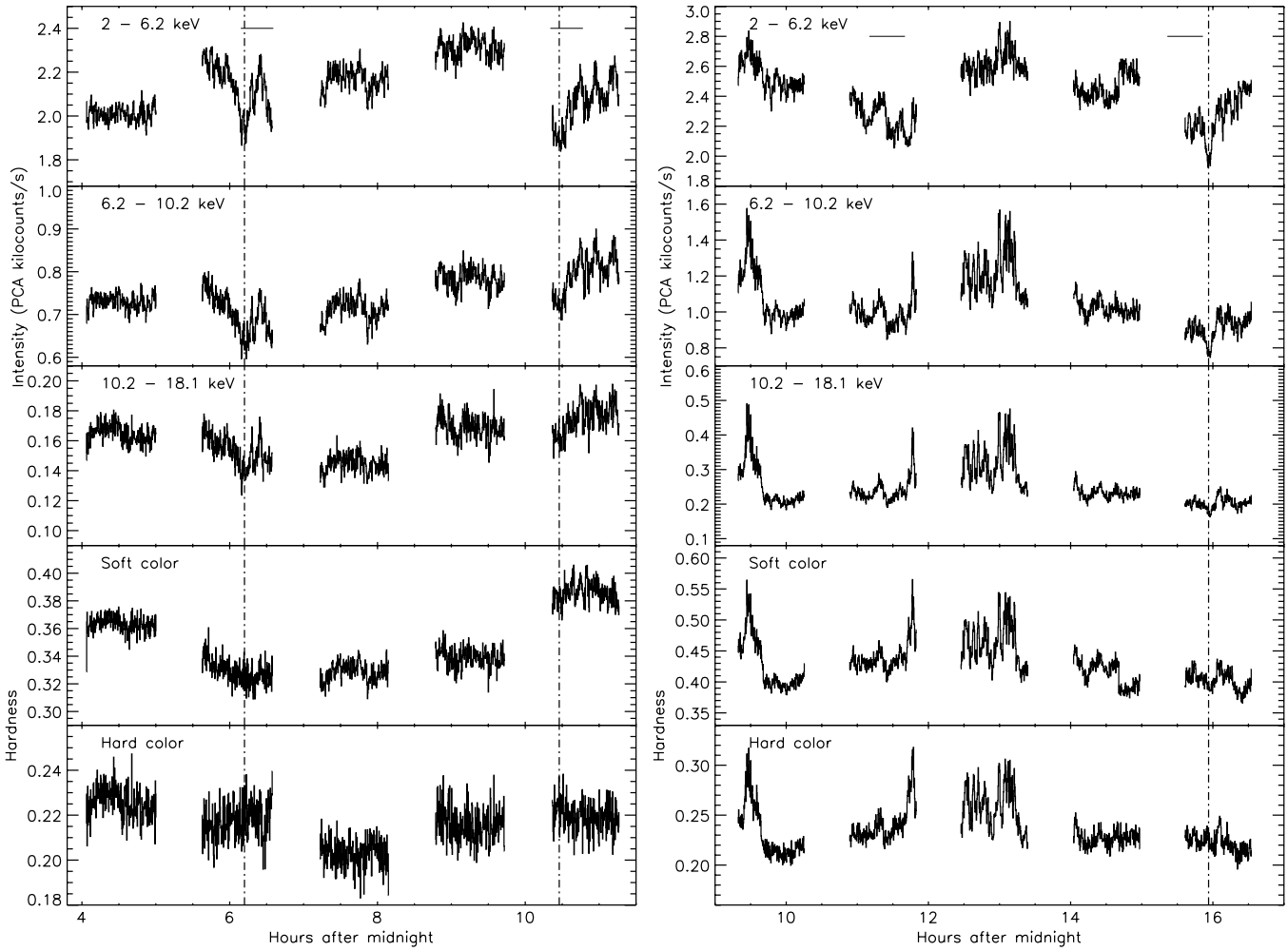

Figure 7. Left: PCA observation of GX 9+9 taken on 2006 June 20 (MJD 53,906; ID 92415-01-01-00). Right: PCA observation of GX 9+9 taken on 2006 September 1 (MJD 53,979; ID 92415-01-02-00). Both time axes are labeled in hours after midnight TT of the day of the observation. The horizontal bars indicate the times of X-ray minimum according to Equation (2). The panels labeled "soft color" and "hard color" are, respectively, the ratio of counts in the 6.2–10.2 keV band to that in the 2–6.2 keV band, and the ratio of counts in the 10.2–18.1 keV band to that in the 6.2–10.2 keV band. The vertical dash-dotted lines mark the center times of notable diplike events.

Table 2
Dip Times and Depths in PCA Data

Figure No.	ObsID	Energy Band (keV)	Centroid Time[a] (hr)	Centroid Time[b] (MJD)	Orbital Phase[c] (cycles)	Depth (fraction)
5	70022-02-01-01	2–6	8.363 ± 0.02	52,395.9195	-0.048 ± 0.095	0.031 ± 0.004
5	70022-02-01-01	2–6	12.548 ± 0.01	52,396.0939	-0.050 ± 0.095	0.041 ± 0.002
6	70022-02-05-00	2–6	0.575 ± 0.01	52,431.4034	0.034 ± 0.092	0.026 ± 0.006
6	70022-02-05-00	2–6	5.328 ± 0.01	52,431.6014	0.168 ± 0.092	0.067 ± 0.008
7(left)	92415-01-01-00	2–6	6.201 ± 0.01	53,906.2584	-0.041 ± 0.053	0.137 ± 0.003
7(left)	92415-01-01-00	6–10	6.212 ± 0.01	53,906.2588	-0.038 ± 0.053	0.172 ± 0.004
7(left)	92415-01-01-00	10–18	6.204 ± 0.02	53,906.2585	-0.040 ± 0.053	0.171 ± 0.007
7(left)	92415-01-01-00	2–6	10.461 ± 0.02	53,906.4359	-0.025 ± 0.053	0.102 ± 0.003
7(left)	92415-01-01-00	6–10	10.461 ± 0.01	53,906.4359	-0.025 ± 0.053	0.114 ± 0.003
7(left)	92415-01-01-00	10–18	10.443 ± 0.05	53,906.4351	-0.029 ± 0.054	0.095 ± 0.004
7(right)	92415-01-02-00	2–6	15.937 ± 0.01	53,979.6640	0.076 ± 0.059	0.098 ± 0.007
7(right)	92415-01-02-00	6–10	15.939 ± 0.01	53,979.6641	0.077 ± 0.059	0.117 ± 0.009
7(right)	92415-01-02-00	10–18	15.940 ± 0.01	53,979.6642	0.077 ± 0.059	0.108 ± 0.013

Notes.
[a] Time relative to the origin in the figure.
[b] Centroid time as a Modified Julian Date.
[c] Computed according to Equation (2). The uncertainty is the root-sum-squared of the 1σ errors in the projection of the ephemeris given in Equation (2) and the time of the dip centroid. The uncertainties in the dip centroid times are small in comparison with the ephemeris uncertainties.

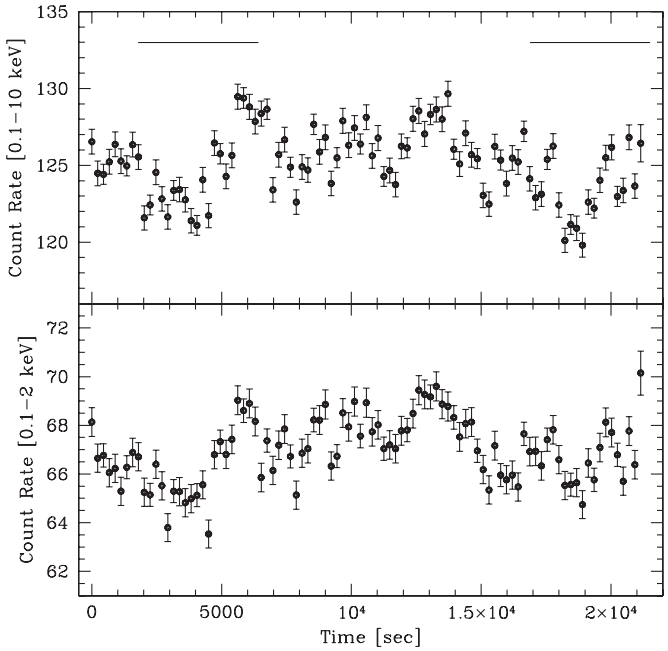

Figure 8. Intensity as a function of time of GX 9+9 as shown by counts in 200 s time bins obtained from the *Chandra* ACIS–HETG observation. Time is referenced to the beginning of the observation at 2000 August 22 05:20:21 (MJD 51778.2225). The horizontal bars indicate the times of X-ray minimum according to Equation (2).

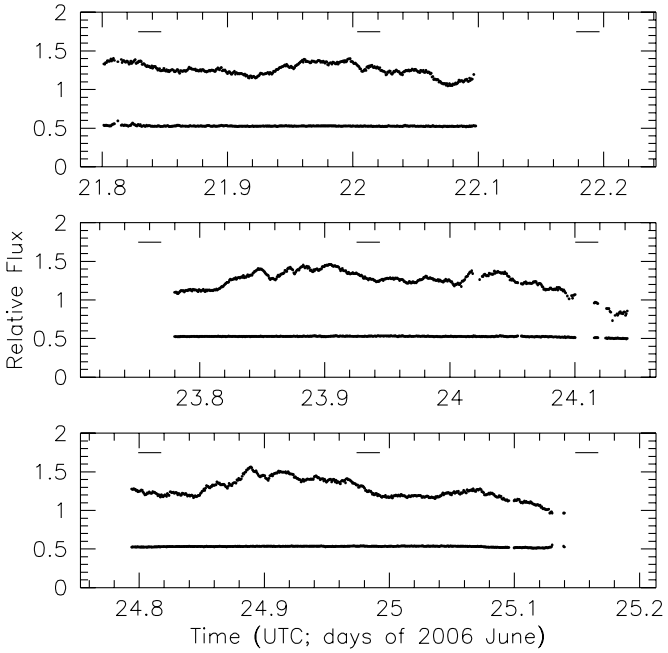

Figure 9. Optical light curves of the optical counterpart of GX 9+9 and a similar brightness check star. The fluxes of the two stars are each shown on an independent relative intensity scale; the scale for the check star was chosen so that its light curves do not overlap with those of the counterpart of GX 9+9. These light curves were created using only those measurements that deviated by less than 0.05 mag from local running averages. One minute average intensities are shown. The observation times have been corrected to the solar system barycenter. The times of X-ray minimum intensity according to the ephemeris in Equation (2) are indicated with horizontal bars. For reference, 2006 June 20 is MJD 53,906.

these observations, and was lowest in the sky near the end of the observations, especially on the nights of June 23–24 and 24–25 (see Figure 9). This also suggests that the use of the

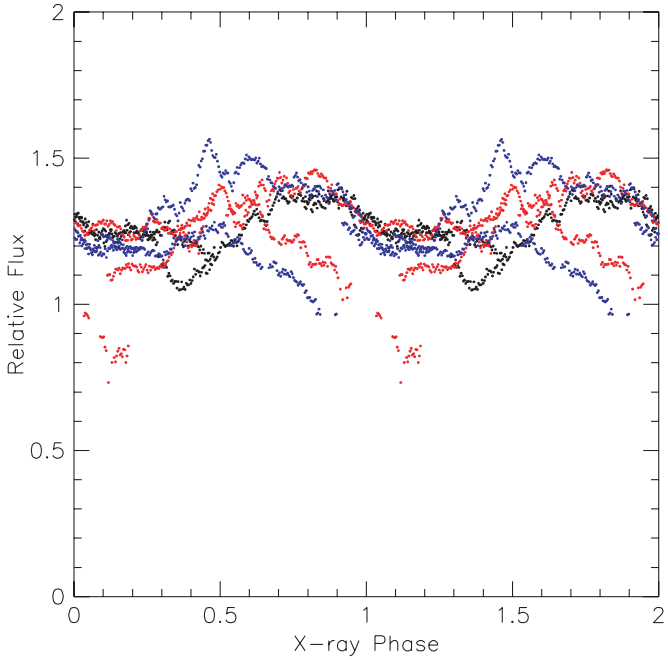

Figure 10. Optical light curves of GX 9+9 from Figure 9 plotted (twice) as a function of X-ray phase determined using Equation (2). The fluxes for each of the three nights (June 21–22, black; June 23–24, red; June 24–25, blue) are shown on a normalized linear scale. The decline at late times of the intensity on the nights of June 23–24 and 24–25 may be an artifact (see the text).

comparison star to normalize the flux may not have removed other slow variations in the intensity of the counterpart of GX 9+9. If we discount the tails of the red and blue curves where they fall below the other photometric results, we find that the variability has a strong periodic component. The light curves roughly suggest that optical minimum comes near X-ray phase 0.2, but the nonperiodic aspects of the light curves do not allow a firm conclusion to be drawn.

From a Lomb–Scargle periodogram of the data, we find the source varies roughly sinusoidally with a period 4.17 ± 0.11 hr, with short-term variability superposed. The amplitude of the 4.19 hr modulation is roughly $\pm 15\%$. This is close to or slightly smaller than that seen in previous observations.

3. DISCUSSION

The long-term ASM light curve of GX 9+9 shows that its intensity has changed slowly over the 12 years that it has been observed. The form of the variations suggest the presence of a periodicity with a period of 1400–1600 days, but the light curve is not well fit by a simple linear function plus a sinusoid. Perhaps the variability is quasi-periodic in nature. Possible causes of the changes include (1) variation in the accretion rate due to the donor star being a long-period variable star that is undergoing small changes in size, (2) the presence of a third star in the system in a $\sim$16 day orbit around the center of mass of the other two stars which produces the variation by dynamical effects on the close pair (e.g., Mazeh & Shaham 1979; Ford et al. 2000; Zdziarski et al. 2007), and (3) the presence of a tilted, precessing accretion disk (although the long period would be hard to understand if this is the correct explanation). In any case, it would certainly be of interest to extend the X-ray light curve by monitoring the intensity for many additional years. It would also be of interest to determine whether similar variation is also manifest in the optical band.

A detailed analysis of the ASM data has revealed significant changes in the amplitude of the orbital (4.19 hr) modulation in the X-ray intensity. When strong, the modulation is characterized by energy-independent reductions in intensity that are limited in phase; the light curves are definitely nonsinusoidal in form.

We used the ASM data to determine an ephemeris for the times of X-ray minimum. Our epoch differs from that of Cornelisse et al. (2007); the epoch in the latter report occurs at a phase of ∼0.24 cycles according to Equation (2). In response to our query, we were informed (R. Cornelisse 2008, private communication) that the epoch of the time of minimum that is explicitly stated in Section 3.1 of Cornelisse et al. (2007) is indeed incorrect but the X-ray phases used for the analyses and figures in that paper actually had been calculated using the correct epoch.

While the modulation is strong (MJD 53,300–54,100), the intensity of GX 9+9 is reduced in comparison to that based on an interpolation from the 2003–2004 time interval to the 2007 time frame. However, the degree of modulation during two similar reduced-intensity time intervals (MJD 50,300–51,100 and MJD 51,700–52,500) was generally low (with the exception of a small part of the latter interval when it was of moderate strength as seen in interval 15 in Figure 3).

PCA data obtained during the two-year interval when the X-ray modulation was strong show evidence of diplike intensity reductions at orbital phases more or less consistent with the ASM folded light curves. The energy independence of the folded ASM light curves (Figure 4) is confirmed by the results in Table 2 which show that the depths of the diplike events seen in the PCA data are roughly independent of photon energy. The intensity of GX 9+9 is generally less variable at low X-ray energies, e.g., below 6 keV, than at higher energies. This random variability tends to mask the diplike reductions at the higher energies. Thus, the reductions are more evident at low X-ray energies. PCA and *Chandra* data obtained prior to this two-year interval show that if diplike events were present, they tended to be rather shallow. The diplike intensity reductions, regardless if they occurred during the two year time interval when the modulation was strong on average or at other times, are relatively limited in phase; they generally lasted less than 0.1 orbital periods. On the whole, the PCA and *Chandra* data suggest that the form of the light curves seen in the ASM data is the result of the superposition of many dips with preferred but varying phases, depths, and widths.

The amplitude of the 4.19 hr modulation in the 2006 optical observations is comparable to that seen in 1999 by Kong et al. (2006), to that seen in 2004 by Cornelisse et al. (2007), and also to that seen in 1987 and 1988 by Schaefer (1990) even though the X-ray modulation strength was much greater around the time of the 2006 observations than at the time of the 1999 or 2004 observations.

The light curves from the 2006 optical observations, which covered just over three orbital cycles, indicate that the time of minimum optical flux is likely around 0.2 cycles after the time of minimum X-ray flux given by Equation (2). However, this conclusion about the optical-to-X-ray phase relationship is not secure because of deviations in the light curves from one cycle to another. The light curves obtained by Kong et al. (2006) from just over four orbital cycles in 1999 present a similar picture; phase zero in their Figures 5 and 6 corresponds (by coincidence) to phase 0.01 ± 0.20 according to our X-ray ephemeris. Note that all four nightly folded light curves in their Figure 6 have minima near phase 0.2. In contrast, Cornelisse et al. (2007) obtained light curves over three orbital cycles in 2004 and concluded that the time of minimum optical flux (in the continuum) corresponded closely to the time of minimum X-ray flux. Cornelisse et al. (2007) did not show the individual light curves nor do we know the precise time they used as the time of minimum X-ray flux. It is possible that the X-ray and optical light curves of GX 9+9 do not maintain a strict phase relationship. Extensive further observations will be needed to resolve this question.

The X-ray intensity reductions in GX 9+9 are grossly similar to the dips in 10 or more LMXBs such as 4U1915−05, X1254−690, EXO 0748−676, X1755−33, or X1746−370 that appear at certain (limited) orbital phases as absorptionlike events. In such dipping sources, the dips do not always occur at precisely the same orbital phases, often exhibit complicated structure, and often are stronger at low energies in a manner that suggests photoelectric absorption. The dips occur with a wide range of depths and can have durations up to as much as 25% or 30% of an orbital period. At one extreme, the source 4U1915−05 has exhibited dips that were essentially 100% deep, showed evidence of photoelectric absorption, and were, in some cases, temporally complex (Walter et al. 1982; White & Swank 1982; Church et al. 1997). At the other extreme, the dips seen in X1755−33 were not much more than 30% deep, had essentially no energy dependence, and, at least in some cases, were relatively simple in their degree of structure (White et al. 1984; Church & Bałucińska-Church 1993). It is common for the characteristics of the dips seen in a given source to vary; see, e.g., Bałucińska-Church et al. (2004) for a discussion of changes in the dipping amplitude for X1746−370, Parmar et al. (1986) and Homan et al. (2003) for reports on dipping activity in EXO 0748−676, and Smale & Wachter (1999) for a report on the entire cessation of dipping for a time in X1254−690.

No evidence of enhanced absorption at low energy is apparent in the folded ASM light curves that show the GX 9+9 dips. This is confirmed by a few dips seen in PCA light curves which also show that the intensity reductions do not have the degree of structure seen in individual orbital cycles in many dippers. However, the characteristics of dips seen in various sources are rather diverse, and the diplike events in GX 9+9 are reminiscent of the dips that were evident in the *EXOSAT* observations of X1755−33 (White et al. 1984; Church & Bałucińska-Church 1993).

The dipping phenomenon has been explained at a general level as due to the occultation of the X-ray source by localized regions of enhanced density relatively far from the orbital plane around the place where the stream of gas from the donor impacts the accretion disk (Lubow & Shu 1976; White & Swank 1982; Walter et al. 1982). According to this general idea, dips will only be evident in those LMXBs whose orbital planes are inclined to the line of sight in a relatively narrow range, namely those not at such high inclinations that our line of sight to the neutron star always intercepts the high-density parts of the disk nor those at such low inclinations that the line of sight is never intercepted by the thick structures in the gas stream/disk collision region. Since the present results on GX 9+9 are similar to those previously seen in X1755−33, they do not suggest extensions of the conventional picture, but they do indicate that GX 9+9 is viewed at relatively high inclination like the other dippers. The energy independence of the dips seen in GX 9+9 may then be the product of different degrees of energy-dependent absorption of multiple emission components such

as discussed by Church & Bałucińska-Church (1993) in the context of X1755−33 rather than the product of high ionization or elemental abundance anomalies (White et al. 1984). However, one should note that there is not at this time a full consensus on the interpretations of the observations of dips especially on the locations and sizes of the emission components and the degree of ionization of the absorbers (e.g., Church & Bałucińska-Church 2004; Church et al. 2005; Díaz Trigo et al. 2006, and references therein).

We thank the anonymous referee for helpful comments. A.T.S. and M.D. acknowledge support from the Spanish Ministry of Science and Technology under grants AYA 2004-02646 and AYA 2007-66887.

REFERENCES

Bałucińska-Church, M., Church, M. J., & Smale, A. P. 2004, MNRAS, 347, 334
Church, M. J., & Bałucińska-Church, M. 1993, MNRAS, 260, 59
Church, M. J., & Bałucińska-Church, M. 2004, MNRAS, 348, 955
Church, M. J., Dotani, T., Bałucińska-Church, M., Mitsuda, K., Takahashi, T., Inoue, H., & Yoshida, K. 1997, ApJ, 491, 388
Church, M. J., Reed, D., Dotani, T., Bałucińska-Church, M., & Smale, A. P. 2005, MNRAS, 359, 1336
Cornelisse, R., Steeghs, D., Casares, J., Charles, P. A., Barnes, A. D., Hynes, R. I., & O'Brien, K. 2007, MNRAS, 380, 1219
Díaz Trigo, M., Parmar, A. N., Boirin, L., Méndez, M., & Kaastra, J. S. 2006, A&A, 445, 179
Ford, E. B., Kozinsky, B., & Rasio, F. A. 2000, ApJ, 535, 385
Hasinger, G., & van der Klis, M. 1989, A&A, 225, 79
Hertz, P., & Wood, K. S. 1988, ApJ, 331, 764
Homan, J., Wijnands, R., & van den Berg, M. 2003, A&A, 412, 799
Jahoda, K., Markwardt, C. B., Radeva, Y., Rots, A. H., Stark, M. J., Swank, J. H., Strohmayer, T. E., & Zhang, W. 2006, ApJS, 163, 401
Kong, A. K. H., Charles, P. A., Homer, L., Kuulkers, E., & O'Donoghue, D. 2006, MNRAS, 368, 781
Levine, A. M., Bradt, H., Cui, W., Jernigan, J. G., Morgan, E. H., Remillard, R., Shirey, R. E., & Smith, D. A. 1996, ApJ, 469, L33
Levine, A. M., & Corbet, R. 2006, ATel, 940, 1
Levine, A. M., Harris, R. J., & Vilhu, O. 2006, ATel, 839, 1
Lubow, S. H., & Shu, F. H. 1976, ApJ, 207, L53
Mayer, W., Bradt, H. V., & Rappaport, S. 1970, ApJ, 159, L115
Mazeh, T., & Shaham, J. 1979, A&A, 77, 145
Parmar, A. N., White, N. E., Giommi, P., & Gottwald, M. 1986, ApJ, 308, 199
Schaefer, B. E. 1990, ApJ, 354, 720
Schulz, N. S., Hasinger, G., & Truemper, J. 1989, A&A, 225, 48
Shivamoggi, V. 2005, B.S. thesis, Massachusetts Inst. of Technology
Smale, A. P., & Wachter, S. 1999, ApJ, 527, 341
Stetson, P. B. 1987, PASP, 99, 191
Stetson, P. B., Davis, L. E., & Crabtree, D. R. 1990, in ASP Conf. Ser. 8, CCDs in Astronomy, ed. G. H. Jacoby (San Francisco, CA: ASP), 289
van der Klis, M. 2006, in Compact Stellar X-ray Sources, ed. W. Lewin & M. van der Klis (Cambridge: Cambridge Univ. Press), 39
Walter, F. M., Mason, K. O., Clarke, J. T., Halpern, J., Grindlay, J. E., Bowyer, S., & Henry, J. P. 1982, ApJ, 253, L67
Weisskopf, M. C., Brinkman, B., Canizares, C., Garmire, G., Murray, S., & Van Speybroeck, L. P. 2002, PASP, 114, 1
White, N. E., Parmar, A. N., Sztajno, M., Zimmermann, H. U., Mason, K. O., & Kahn, S. M. 1984, ApJ, 283, L9
White, N. E., & Swank, J. H. 1982, ApJ, 253, L61
Wijnands, R., van der Klis, M., & van Paradijs, J. 1998, in Proc. IAU Symp. 188, The Hot Universe, ed. K. Koyama, S. Kitamoto, & M. Itoh (Dordrecht: Kluwer), 370
Zdziarski, A. A., Wen, L., & Gierliński, M. 2007, MNRAS, 377, 1006